

DISTANCES TO SUPERNOVA REMNANTS G20.4 + 0.1, G24.7 – 0.6, G28.6 – 0.1 AND  
G42.0 – 0.1 AND NEW MOLECULAR CLOUD ASSOCIATIONS

S. RANASINGHE AND D.A. LEAHY<sup>1</sup>

<sup>1</sup>*Department of Physics & Astronomy, University of Calgary, Calgary, Alberta T2N 1N4, Canada*

(Received; Accepted; Published)

Submitted to MNRAS

ABSTRACT

Accurate distances to supernova remnants (SNRs) are crucial in determining their size, age, luminosity and evolutionary state. To determine distances, we chose four SNRs from the VLA Galactic Plane Survey (VGPS) for extraction of HI absorption spectra. Analysing HI absorption spectra, <sup>13</sup>CO emission spectra, and HI and <sup>13</sup>CO channel maps, kinematic velocities (or their limits) to the four SNRs were calculated. The four SNRs are probably associated with molecular clouds and the new distance to G20.4 + 0.1, G24.7 – 0.6, G28.6 – 0.1 and G42.0 – 0.1 are  $7.8 \pm 0.2$  kpc,  $3.8 \pm 0.2$  kpc,  $9.6 \pm 0.3$  kpc and  $3.5 \pm 0.4$  kpc, respectively.

*Keywords:* ISM: supernova remnants – radio continuum: ISM – radio lines: ISM

## 1. INTRODUCTION

For the study of a supernova remnant (SNR), distance as a basic physical parameter is crucial in order to determine its size, luminosity and age. SNRs are an important source of energy and element-enriched ejecta input for the interstellar medium (ISM). They are associated with several highly active phenomena including Anomalous X-ray Pulsars (AXP), Soft Gamma-ray Repeaters (SGR), Pulsar Wind Nebulae (PWNe) and non-thermal X-ray and very high energy emission. Distance determination of a SNR leads to association with other objects and constrains the mass range of the progenitor star and type of supernova resulting in the remnant.

However, determination of the distances to SNRs has been a difficult task. The most common method of obtaining distances is by analysing HI absorption spectra. Due to observational constraints, constructing reliable HI absorption spectra has been difficult in the past. However, with recent improvements in observations with better sensitivity and higher resolution, the determination of accurate distances to SNRs have become possible.

In this paper, we use the step-by-step process described by [Ranasinghe & Leahy \(2017\)](#) to determine distances to SNRs. We construct HI absorption spectra using the method developed by [Leahy & Tian \(2010\)](#) and analyse HI absorption spectra,  $^{13}\text{CO}$  emission spectra and the HI and CO channel maps to obtain distances.

In Section 2, we discuss the data and software used for this analysis, construction of HI absorption spectra, determination of kinematic distances and error analysis. The results for the four selected SNRs are presented in Section 3 and in Section 4 a summary is given.

## 2. DATA ANALYSIS

### 2.1. Data and Software

We extract the 1420 MHz radio continuum and HI-line emission data from the VLA (Very

Large Array) Galactic Plane Survey (VGPS) ([Stil et al. 2006](#)). The  $^{13}\text{CO}$  spectral line data are obtained from the Galactic Ring Survey of the Five College Radio Astronomical Observatory (FCRAO) 14 m telescope ([Jackson et al. 2006](#)). We construct source and background spectra using MEANLEV, a software program in the DRAO EXPORT package. This program allows one to extract on and off spectra defined by spatial boundaries and by user-specified threshold  $T_B$  levels.

### 2.2. Construction of HI Absorption Spectra and kinematic distances

To construct HI absorption spectra we adopt the method presented by [Leahy & Tian \(2010\)](#). We begin with the equation of radiative transfer  $\frac{dI_\nu}{ds} = j_\nu - \kappa_\nu I_\nu$ , where  $I_\nu$  is the specific intensity,  $ds$  is the thickness of a slab of medium along the line-of-sight (LOS),  $j_\nu$  is the emission coefficient and  $\kappa_\nu$  is the linear absorption coefficient. From the radiative transfer equation, it follows the HI absorption spectrum is given by:

$$e^{-\tau_\nu} - 1 = \frac{T_{B,\text{on}}(\nu) - T_{B,\text{off}}(\nu)}{T_{B,\text{on}}^C - T_{B,\text{off}}^C}, \quad (1)$$

where  $T_B$  is the brightness temperature, the ‘on’ spectrum is the spectrum towards the source and the ‘off’ spectrum is the spectrum towards the background. A derivation of equation 1 is given by [Leahy & Tian \(2010\)](#). The optical depth vs. frequency (or equivalently radial velocity,  $\nu$ )  $\tau_\nu$ , is the HI absorption spectrum and is plotted here as  $e^{-\tau_\nu}$ .

From the HI absorption spectrum, the radial velocity where the absorption occurs can be identified and therefore, the distance to the object of interest can be determined. Assuming circular rotation, the radial velocity is given by:

$$V_r = R_0 \sin(l) \left( \frac{V(R)}{R} - \frac{V_0}{R_0} \right), \quad (2)$$

where  $l$  is the galactic longitude and  $V(R)$  is the orbital velocity at the Galacto-centric dis-

tance  $R$  (Kwee et al. 1954). The rotation curve provides  $V(R)$  for any  $R$ , hence  $V(R)/R$ , and thus  $R$  can be found from equation 2. The relation between distance,  $d$ , to the object from the Sun, in the direction of Galactic longitude ( $l$ ) and the Galacto-centric distance  $R$  is given by  $R^2 = R_0^2 + d^2 - 2R_0d \cos(l)$ , which has solution

$$d = R_0 \cos(l) \pm \sqrt{R^2 - R_0^2 \sin^2(l)}. \quad (3)$$

The existence of two possible distances for locations inside the solar circle, corresponding to the plus and minus signs above, is called the Kinematic Distance Ambiguity (KDA).

For each SNR, the brightest continuum regions were chosen for the source or ‘on’ position. The background regions or ‘off’ positions were chosen by examining HI channel maps to minimize HI features that could either lie in the source or background regions coincidentally, yielding false HI absorption features unrelated to the SNR. Using MEANLEV allows the source and background to be close to each other or adjacent.

The  $^{13}\text{CO}$  emission spectra were extracted using the same source and background regions as for the HI spectra. An investigation of the  $^{13}\text{CO}$  channel maps indicates whether a molecular cloud might be associated or interacting with a SNR. For our analysis, the edge of the radio emission was taken as the border of the SNR and the reality of morphological association with molecular clouds was judged by eye. For each SNR, there may be a more than one overlapping or adjacent molecular cloud. If there are any maser or broad-line molecular cloud associations from the literature, we consider that to be an argument strengthening a particular association and reject all others, including any other morphological alignments.

To determine distance to an SNR from its radial velocity, an accurate Galactic rotation curve is essential. We have adopted the Universal Rotation Curve (URC) of Persic et al.

(1996) and the parameters given by Reid et al. (2014) which are valid for the region of the Galaxy under study. The parameters include the distance to the Galactic center of  $R_0 = 8.34 \pm 0.16$  kpc and the orbital velocity of the sun of  $V_0 = 241 \pm 8$  km s $^{-1}$ . The other URC parameters from Reid et al. (2014) are  $a = 1.5$ ,  $R_{\text{opt}} = R_0 \cdot (0.90 \pm 0.006)$ ,  $V(R_{\text{opt}}) = 241 \pm 8$  and  $\beta = 0.72$ .

### 2.3. Error Analysis

Once HI absorption spectra for the SNRs were constructed, we take the  $2\sigma$  noise level as an indicator of reliability for any HI absorption feature. The  $2\sigma$  noise level was calculated from the absorption spectrum using those velocities where there is no HI emission in the source and background spectra. Given an HI absorption spectrum, we investigated the individual HI channel maps to verify whether each absorption feature was real or an artifact. We based our final conclusions by comparing the HI channel maps and the HI spectra.

In some cases, we see calculated values of  $e^{-\tau} < 0$  or  $e^{-\tau} > 1$  (e.g. the blue line in the lower half of the top two panels of Figure 14). These features are due to HI emission which is in one of, but not both, the background region or source region. For example, Figure 15 top panel shows a case where there is excess HI emission, i.e. excess  $T_{B,\text{off}}$ , in the background region (the part of the red box outside the SNR). This shows up in the HI spectrum (see equation 1) as a negative contribution to  $e^{-\tau}$ , i.e. a false absorption feature. Figure 15 bottom panel shows a case where there is excess HI emission (excess  $T_{B,\text{on}}$ ) in the source region (the part of the red box inside the SNR). This excess HI emission in the source region results in a positive contribution to  $e^{-\tau}$  (equation 1), and, if strong enough, yields a value  $e^{-\tau} > 1$ . Excess HI emission in the background region, if strong enough, can yield a value  $e^{-\tau} < 0$ . Disregarding a feature in an HI spectrum was done after thoroughly in-

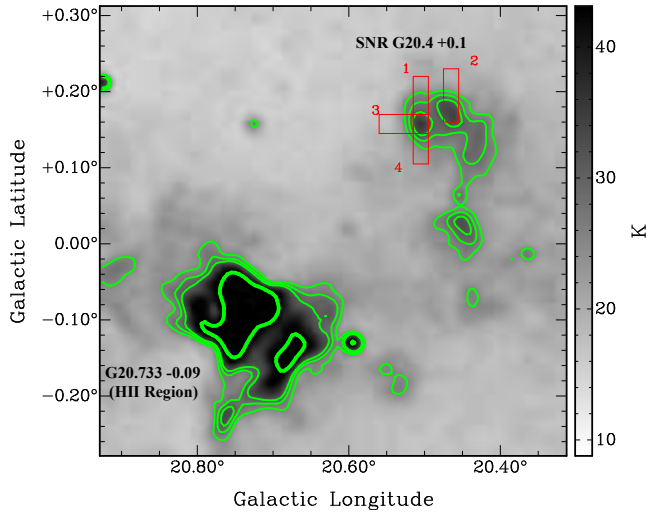


**Figure 1.** SNR G20.4 + 0.1 1420 MHz continuum image with contour levels (green) at 25, 28, 31 and 50 K. The red boxes are the areas used to extract HI and  $^{13}\text{CO}$  source and background spectra.

vestigating the HI channel maps.

The error estimates for the distances were done as follows. Because the equations to determine distance from radial velocities are non-linear, we calculated a set of distances for our best fit parameters and for upper and lower limits of the parameters. The three parameters are  $R_0$ ,  $V_0$  and observed radial velocity  $V_r$ , resulting in a set of  $3^3 = 27$  parameters and distances. Here the errors for  $R_0$  and  $V_0$  were taken from Reid et al. (2014) ( $\pm 0.16$  kpc for  $R_0$  and  $\pm 8$  km s $^{-1}$  for  $V_0$ ). The measurement error in  $V_r$  was taken as  $\pm 2.4$  km s $^{-1}$  based on the channel maps. As an estimate of the peculiar gas motion we take 4.7 km s $^{-1}$  based on the difference of measured tangent point velocities and the URC. Added in quadrature the net error in  $V_r$  is 5.3 km s $^{-1}$ . The standard deviation of the calculated distances (27 values per SNR) yields our estimate of the error in the distance.

### 3. RESULTS

#### 3.1. G20.4 + 0.1

Also known as G20.47 + 0.16, the SNR was first discovered by Brogan et al. (2006) using the 90 cm multi-configuration VLA survey of

the Galactic plane. The SNR has a spectral index that is  $\sim 0.1$  with a high degree of uncertainty. The  $7' \times 7'$  SNR is in a complex region with possible overlapping HII regions and radio sources. Figure 1 shows 1420 MHz image of G20.47 + 0.16. For this SNR there is no known distance, but the HII region G20.733 – 0.09, to the lower-left of the SNR, is placed at a distance of 11.9 kpc (Quireza et al. 2006).

Extracting HI absorption spectra for the SNR was difficult due to random HI clouds confusing the separation of the source and background. The best results were obtained using the brightest region as the source with three different background regions (see regions 1, 3 and 4 in Figure 2). We investigated the HI channel maps to verify or falsify features in the absorption spectra.

Inspecting the HI spectra, it is seen that there may be absorption present up to the tangent point. This conclusion is strengthened by examining the HI channel maps (Figure 3 bottom panel). At a radial velocity of  $\sim 116$  km s $^{-1}$  (see lower panel of Figure 4), the absorption feature matches the shape of the continuum intensity. Hence the SNR is at least at a distance of the tangent point, 7.8 kpc. The absorption feature seen at  $\sim -35$  km s $^{-1}$  in regions 1, 2 and 4 does not well match with the SNR continuum intensity (Figure 3 top panel). This leads to the conclusion that the feature is not true absorption but rather is caused by HI in the background regions. Therefore the upper limit is the far-side of the solar circle of 15.6 kpc.

Figure 4 shows the  $^{13}\text{CO}$  channels near the tangent point velocity (120 km s $^{-1}$ ). It is seen that there is a molecular cloud with boundary that closely matches the northern border of the SNR. The conclusion is that there is a molecular cloud at the tangent point probably associated with the SNR. This observation constrains the distance to be very nearly the tangent point

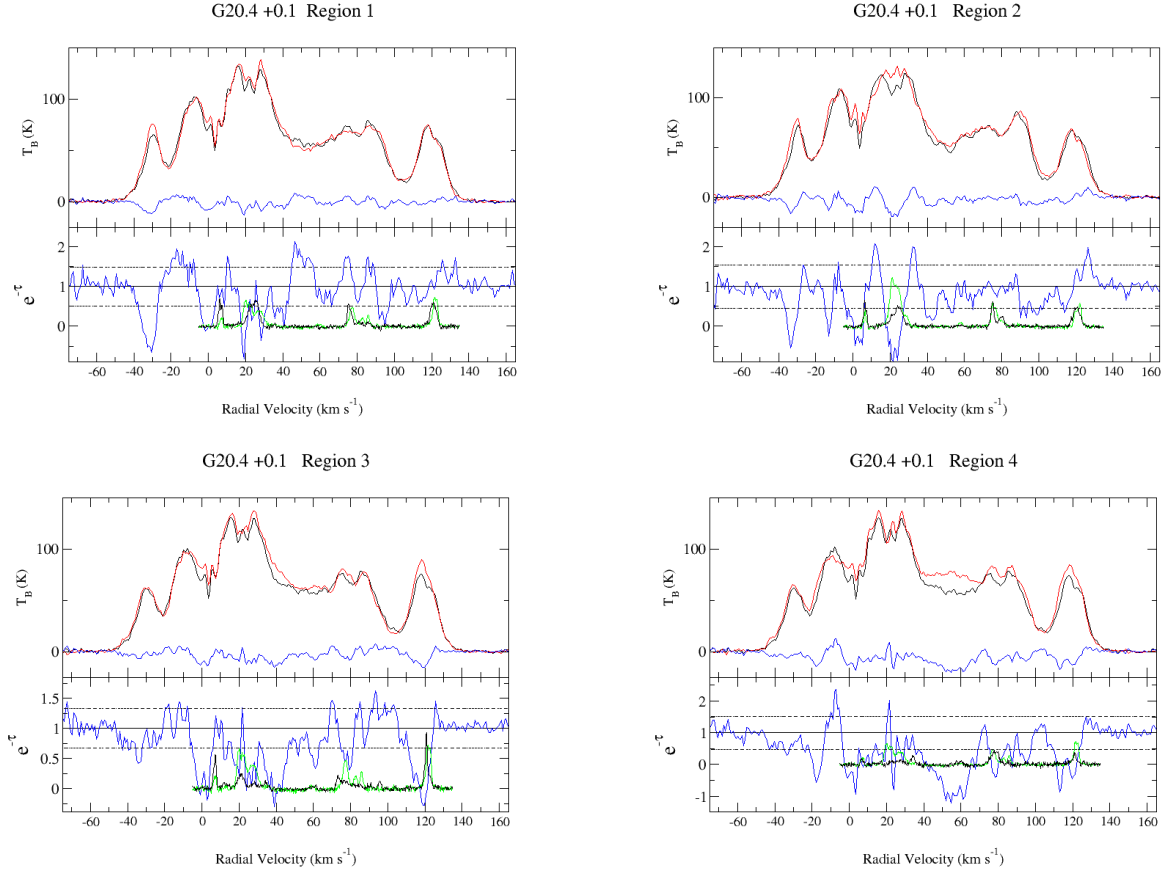


**Figure 2.** G20.4 + 0.1 spectra: The top two left panels are for Region 1, the lower two left panels are for Region 2, the top two right panels are for Region 3, and the lower two right panels are for Region 4. The top panel in each pair shows HI emission spectra: source spectrum (black), background spectrum (red) and difference (blue). The bottom panel in each pair gives the HI absorption spectrum (blue), the  $^{13}\text{CO}$  source spectrum (green) and the  $^{13}\text{CO}$  background spectrum (black). The dashed line is the  $\pm 2\sigma$  noise level of the HI absorption spectrum.

distance, 7.8 kpc.

### 3.2. G24.7 – 0.6

The SNR was first observed by ? at 408 MHz and 5000 MHz. They reported the partial shell appearing at both frequencies and a spectral index of 0.49. Based on the 1465 MHz data of G24.7 – 0.6, the estimated diameter is  $\sim 18'$  for the incomplete shell (Dubner et al. 1993). Koo & Heiles (1991) discussed the possibility of a velocity HI gas between 143 and 176  $\text{km s}^{-1}$  implying an expanding HI shell. However, since the emitting region is much larger than the SNR, the emission is more likely to be

associated with the nearby HII region complex. The distance to the remnant has not been estimated.

Figure 5 shows 1420 MHz image of G24.7–0.6. Regions 1 and 2 were chosen as for extraction of HI and CO spectra, shown in Figure 6. The HI spectra indicate absorption up to the tangent point. However the individual HI channel maps indicate the absorption features between  $\sim 100$  and  $\sim 120 \text{ km s}^{-1}$  to be false, so the SNR is on the near side of the tangent point. E.g. Figure 7 (bottom panel) shows that the shape of the depression in HI emission at  $110 \text{ km s}^{-1}$  does not correlate with the continuum intensity, thus the absorption features are caused excess emission



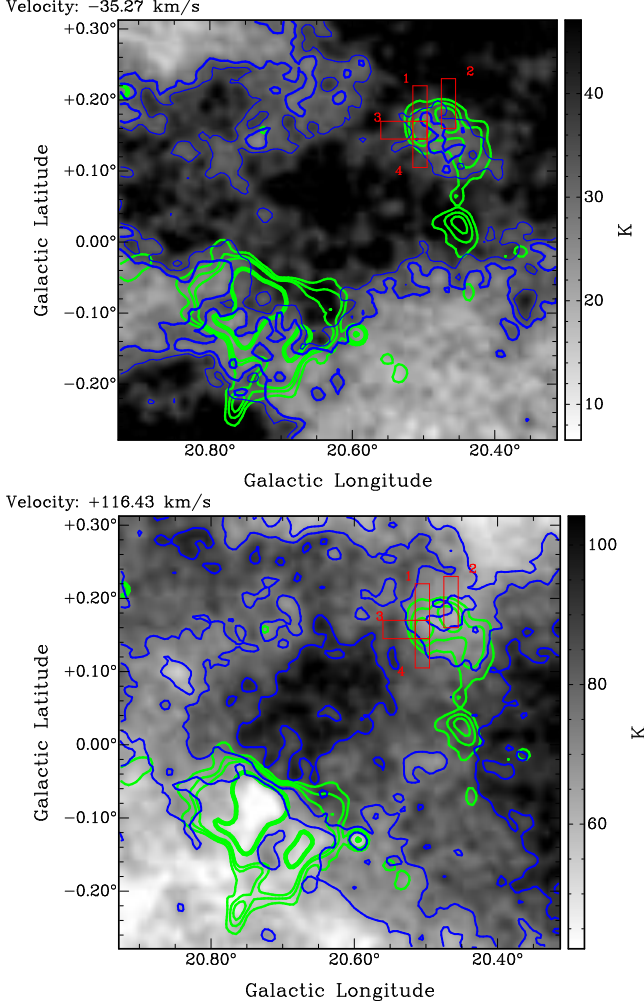


**Figure 3.** G20.4+0.1 HI channel maps  $-35.27$  and  $+116.43$   $\text{km s}^{-1}$ . The HI contour levels (blue) are at 30 and 33 K for the channel map  $-35.27$   $\text{km s}^{-1}$  and 64, 75 and 80 for the channel map  $+116.43$   $\text{km s}^{-1}$ . The continuum contour levels (green) are at 25, 28, 31 and 50 K.

in the background regions. Absorption features are seen in the HI absorption spectrum between velocities of  $48 \simeq$  and  $65 \simeq$   $\text{km s}^{-1}$ . Figure 7 (top panel) shows the HI channel map for  $64$   $\text{km s}^{-1}$ . In this case, the depression in HI emission coincides with the brightest continuum emission, verifying that the depression is caused by absorption. The highest velocity with real HI absorption is  $64$   $\text{km s}^{-1}$ . Figure 8) shows  $^{13}\text{CO}$  channel maps at  $60$  to  $62$   $\text{km s}^{-1}$ . There is a good match between the edge of the molecular cloud and the

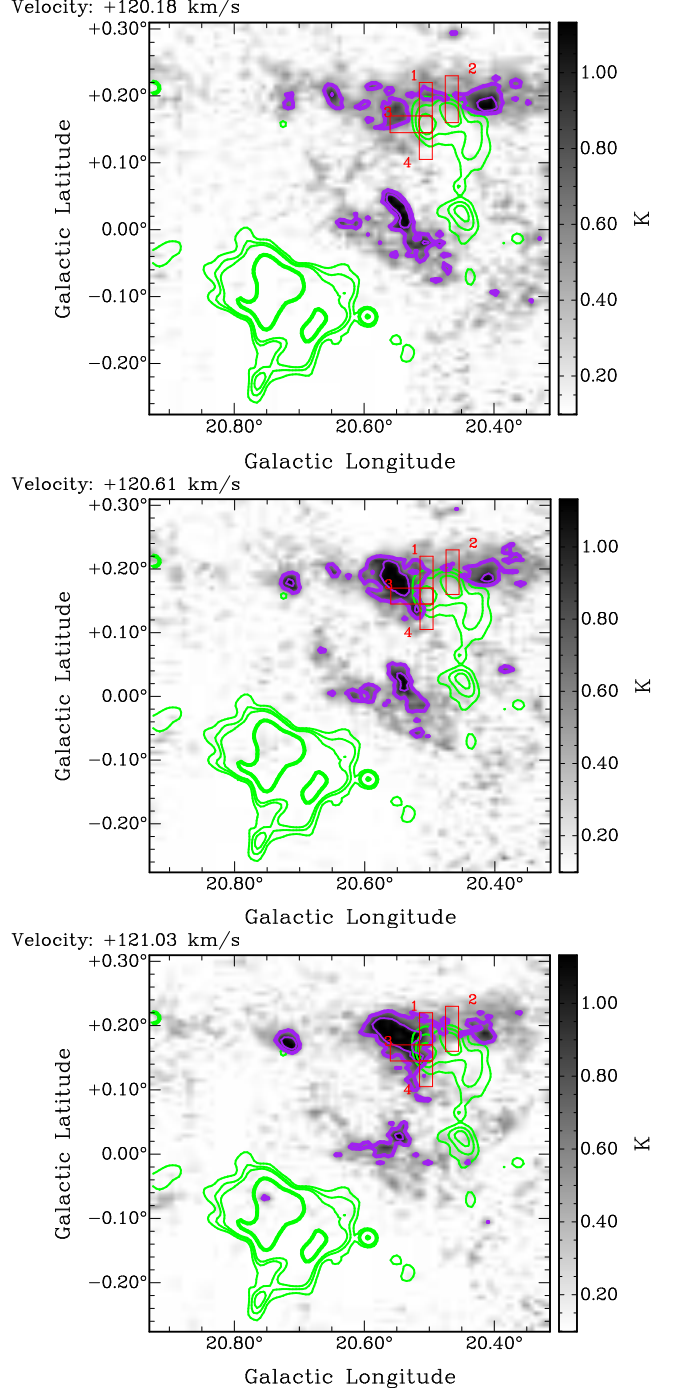


**Figure 4.** G20.4+0.1  $^{13}\text{CO}$  channel maps  $+120.6$  to  $+121.03$   $\text{km s}^{-1}$ . The  $^{13}\text{CO}$  contour levels (purple) are at 0.6 and 1 K. The continuum contour levels (green) are at 25, 28, 31 and 50 K.

north-western border of the SNR: the SNR appears to be in contact with the molecular cloud. Thus there is a probable association of the SNR

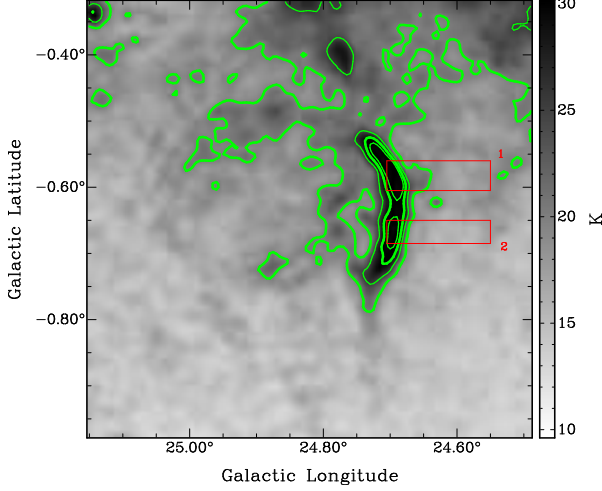


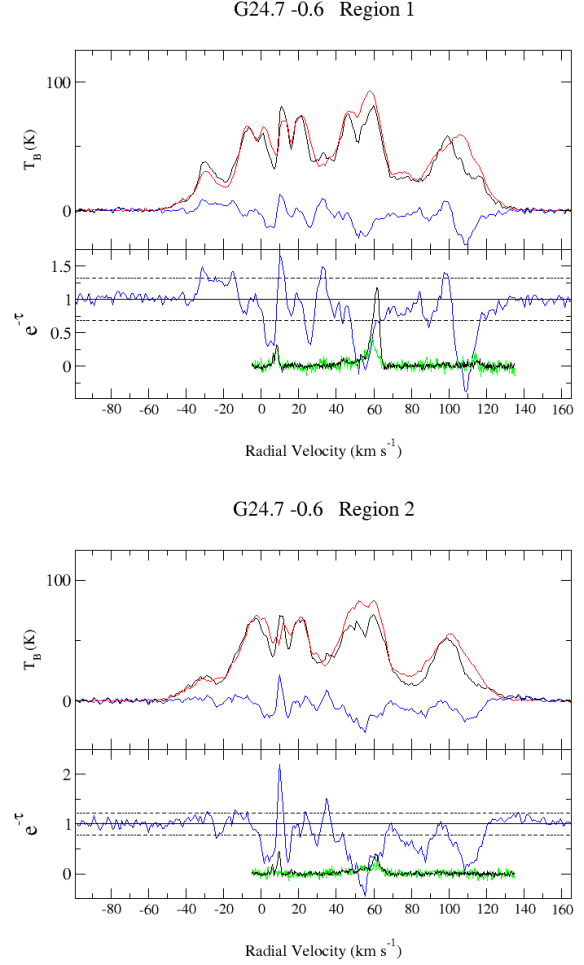
**Figure 5.** SNR G24.7 – 0.6 1420 MHz continuum image with contour levels (green) at 20, 25, 30 and 35 K.

with the molecular cloud at  $\sim 60$  to  $64 \text{ km s}^{-1}$ . For the distance estimation, we use a velocity of  $V_r = 60.67 \text{ km s}^{-1}$ , consistent with the both HI absorption and molecular cloud velocity. Therefore, we place the SNR at the near-distance of 3.8 kpc.

### 3.3. G28.6 – 0.1

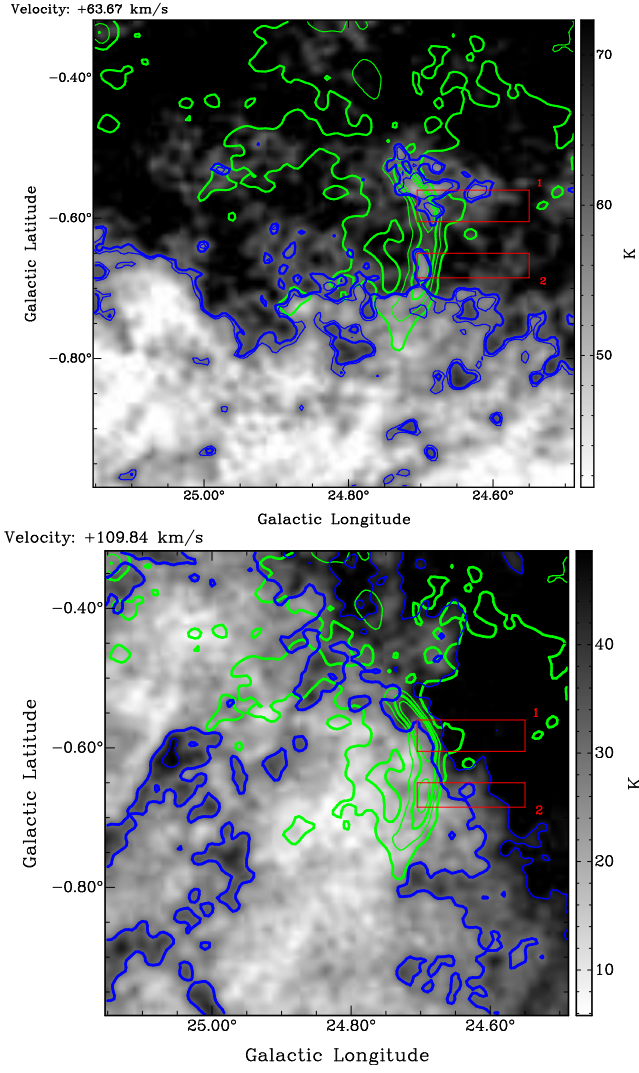
G28.6 – 0.1 is a SNR  $13' \times 9'$  in size (Green 2014) in the G28.60 – 0.13 complex. Helfand et al. (1989) obtained preliminary classifications for most of the objects in this complex. Figure 9 shows the region of the SNR and shows the labels (C, F, G) of the radio sources adopted by Helfand et al. (1989). The X-ray morphology for AX J1843.8 – 0.352 has an elliptical shape with a mean diameter of  $10'$  (Bamba et al. (2001)). AX J1843.8 – 0.352 is a shell-like SNR which emits predominantly synchrotron X-rays from the shell. Bamba et al. (2001) suggested that the non-thermal radio sources C and F, with spectral indices of  $\sim 0.5$  and  $\sim 0.6$  respectively, are associated with the SNR. Object G has a flat radio spectrum and is likely an unrelated HII region. They estimated the SNR distance to be 6 - 8.5 kpc based on the X-ray column density.

Figure 10 shows the HI and CO spectra which



**Figure 6.** G24.7 – 0.6 spectra: The top two panels are for Region 1, the lower two panels are for Region 2. The top panel in each pair shows HI emission spectra: source spectrum (black), background spectrum (red) and difference (blue). The bottom panel in each pair gives the HI absorption spectrum (blue), the  $^{13}\text{CO}$  source spectrum (green) and the  $^{13}\text{CO}$  background spectrum (black). The dashed line is the  $\pm 2\sigma$  noise level of the HI absorption spectrum.

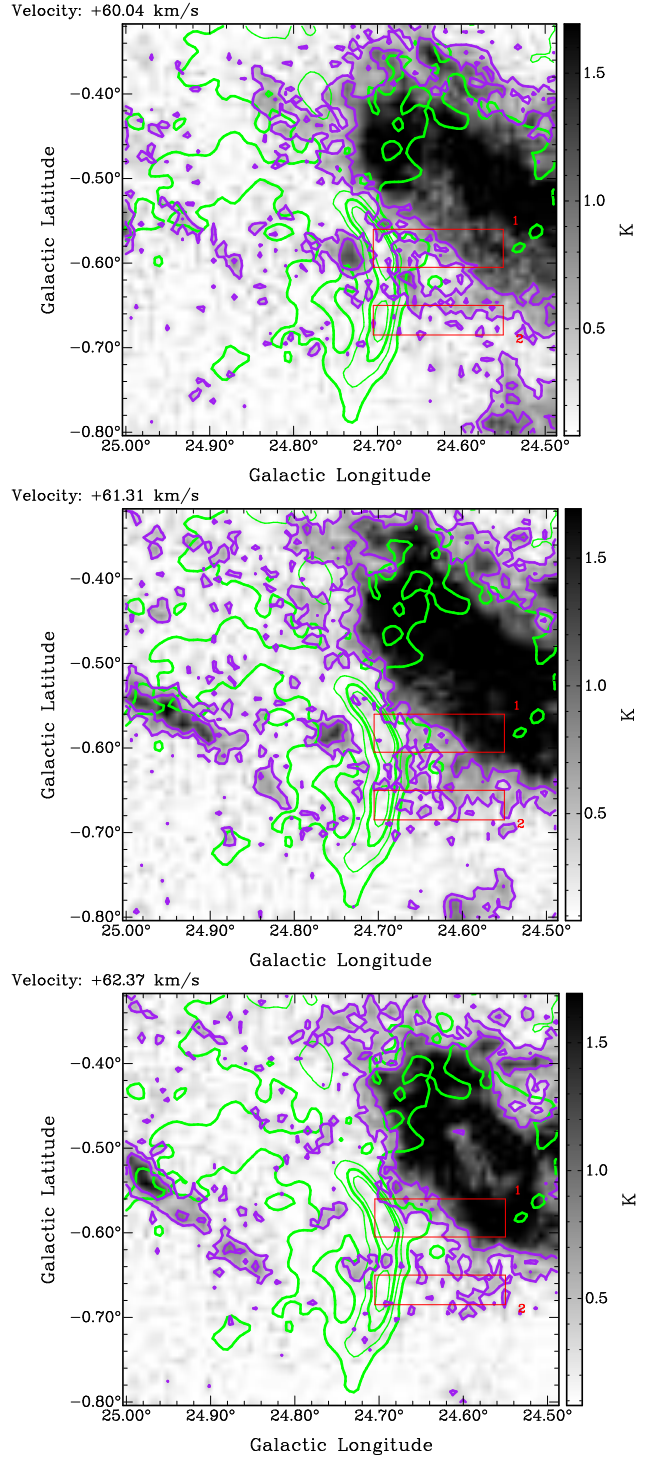
were extracted for regions 1, 2, and 3 (the red boxes in Figure 9). The HI absorption spectra for the SNR regions 1 and 2 show absorption up to the tangent point velocity of  $\sim 108 \text{ km s}^{-1}$ . Figure 11 shows that the HI absorption features closely match the continuum intensity for regions 1 and 2, thus real absorption. Thus the SNR is located beyond the tangent point



**Figure 7.** G24.7 - 0.6 HI channel map +63.67 km s<sup>-1</sup>. The HI contour levels (Blue) are at 58 and 60 K. The continuum contour levels (green) are at 20, 25, 30 and 35 K.

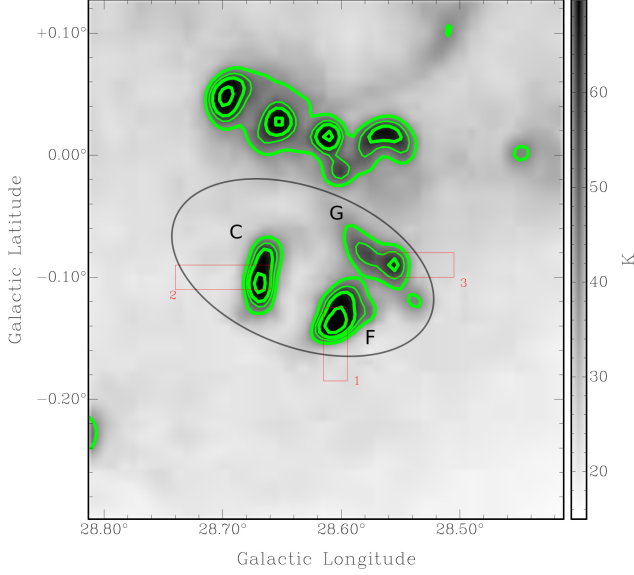
distance of 7.3 kpc. The HII region (source G in Figure 9) does not show real absorption to the tangent point. Thus the HII region is on the near side of the tangent point and unrelated to the SNR. The channel maps also show that the HI absorption features at negative velocities are false features and correspond to excess HI emission in the background regions. Therefore the upper limit of the SNR distance is far-side of the solar circle.

Figure 12 shows the <sup>13</sup>CO channel maps between 84 and 88 km s<sup>-1</sup>. These show a molec-



**Figure 8.** G24.7 - 0.6 <sup>13</sup>CO channel maps +60.04 to +62.37 km s<sup>-1</sup>. The <sup>13</sup>CO contour levels (purple) are at 0.4 and 0.8 K. The continuum contour levels (green) are at levels (green) are at 20, 25, 30 and 35 K.





**Figure 9.** SNR G28.6 – 0.1 1420 MHz continuum image with contour levels (green) at 40, 50, 60 and 80 K. The ellipse is the approximate extent in X-rays of AX J1843.8 – 0.352 given by (Bamba et al. 2001).

ular cloud which appears to surround the radio source F. The morphology of the cloud suggests interaction with the SNR at its lower-right border and not with the HII region (G in Figure 9). The central velocity of the molecular cloud of  $86 \text{ km s}^{-1}$  yields a distance of 9.6 kpc to the SNR.

### 3.4. G42.0 – 0.1

Kaplan et al. (2002) reported on the irregularly shaped SNR, G42.0 – 0.1. Alves et al. (2012) confirmed the synchrotron nature of the SNR. Figure 13 shows the 1420 MHz continuum image of the SNR. The brightest part of the SNR in the continuum images is  $\sim 26 \text{ K}$  and is in an area surrounded by HII regions. The southern protruding region (G42.905 – 0.123) (at  $l=41.90^\circ$ ,  $b=-0.10^\circ$ , see ) was identified as

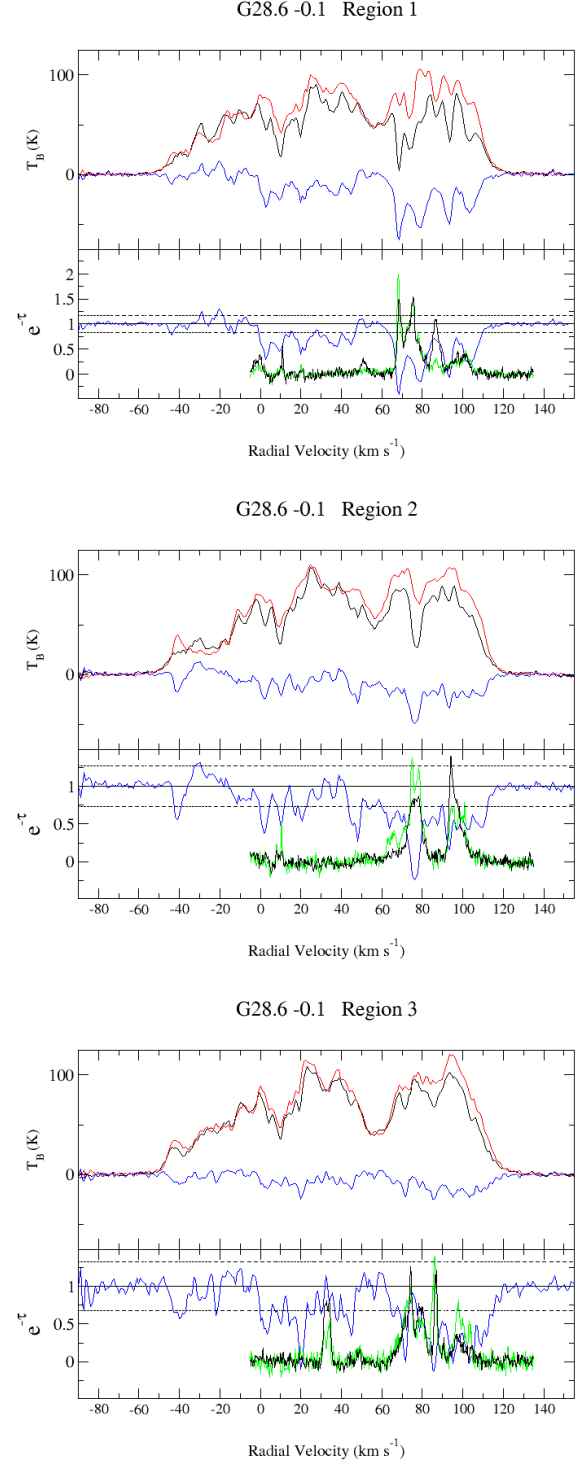


**Figure 10.** G28.6 – 0.1 spectra: The top two panels are for Region 1, the middle two panels are for Region 2, and the lower two panels are for Region 2. The top panel in each pair shows HI emission spectra: source spectrum (black), background spectrum (red) and difference (blue). The bottom panel in each pair gives the HI absorption spectrum (blue), the  $^{13}\text{CO}$  source spectrum (green) and the  $^{13}\text{CO}$  background spectrum (black). The dashed line is the  $\pm 2\sigma$  noise level of the HI absorption spectrum.

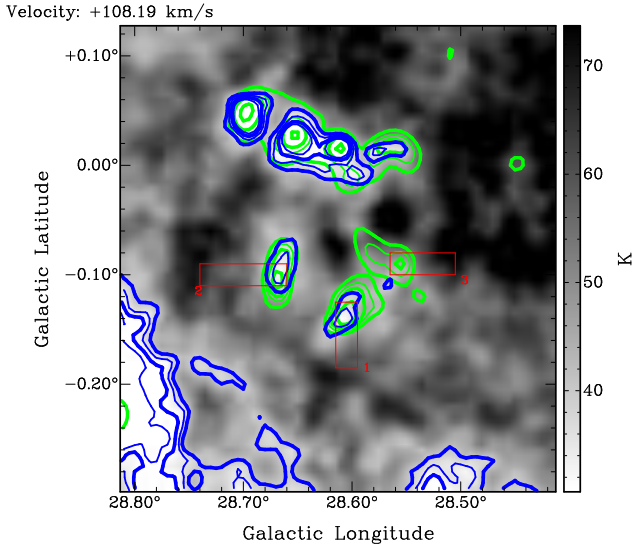


**Figure 11.** G28.6 – 0.1 HI channel map +108.19 km s<sup>-1</sup>. The HI contour levels (Blue) are at 25, 30, 35 and 40 K. The continuum contour levels (green) are at 40, 50, 60 and 80 K.

an HII region based on its radio recombination line at  $18.1 \pm 2.7$  km s<sup>-1</sup> by Lockman et al. (1996). Thus the SNR likely consists of the small (3.6 arcminute diameter) northern bright region only.

Figure 14 shows the HI and CO spectra. Region 1 covers the SNR and region 2 covers the HII region G42.905 – 0.123 (see Figure 13). The SNR spectrum indicates absorption centred on 75 km s<sup>-1</sup>, extending up to about 80 km s<sup>-1</sup>, nearly the tangent point velocity. However the HI channel maps (Figure 15, top panel) show that the 75 km s<sup>-1</sup> feature is not absorption but caused by excess HI emission in the background region. There is good evidence of real absorption at 51.30 km s<sup>-1</sup> (Figure 15, middle panel), where the deficit of HI emission is well correlated with the continuum emission from the SNR. By inspecting the HI channel maps, all absorption features seen in the HI spectrum at the negative velocity range were found to coincide with HI emission in the background region. The features seen at  $e^{-\tau} > 1$  in the SNR HI spectrum (top panel of Figure 14) were found to be caused by excess HI emission in the

source region. As an example, Figure 15 (bottom panel) shows the HI channel map at -38 km s<sup>-1</sup>. The excess emission in the source region causes the  $e^{-\tau} > 1$  feature in the HI spectrum. The conclusion is that the SNR is located at the near-distance corresponding to radial velocity  $v_r \approx 53$  km s<sup>-1</sup>.

Figure 16 shows the <sup>13</sup>CO channel maps for 54-55 km s<sup>-1</sup>. The molecular cloud northern edge follows closely the southern edge of the radio continuum emission from the SNR, which is good evidence of a molecular cloud associated with G42.00.1. Furthermore, the velocity of 55 km s<sup>-1</sup> is consistent with the HI absorption results, yielding a distance of 3.5 kpc.

The HII region spectrum (Figure 14 lower two panels) was compared to the HI channel maps. We found no reliable absorption features and no evidence of HI absorption up to the tangent point. Lockman et al. (1996) gave a recombination line velocity of  $18.1 \pm 2.7$  km s<sup>-1</sup> for this HII region. This is different than the 55 km s<sup>-1</sup> SNR velocity, thus the HII region is not associated with the SNR.

#### 4. DISCUSSION AND CONCLUSION

For the four SNRs studied here, we have found probable molecular cloud associations. For each SNR, this allowed narrowing the range of possible radial velocities to a value consistent with that of the associated molecular cloud. The HI absorption spectra and HI channel maps allowed resolution of the Kinematic Distance Ambiguity. The resulting radial velocities, distances and uncertainties in distances for the four SNRs are given in Table 1.

With the distances for the SNRs, we know the sizes and can estimate their evolutionary states. The mean radius in the 1420 MHz radio continuum image is taken as the shock wave radius,  $R$ . For each SNR, we apply a basic Sedov model (Cox (1972)) because we don't have enough data to justify more complex models. The shock wave radius in the Sedov stage is

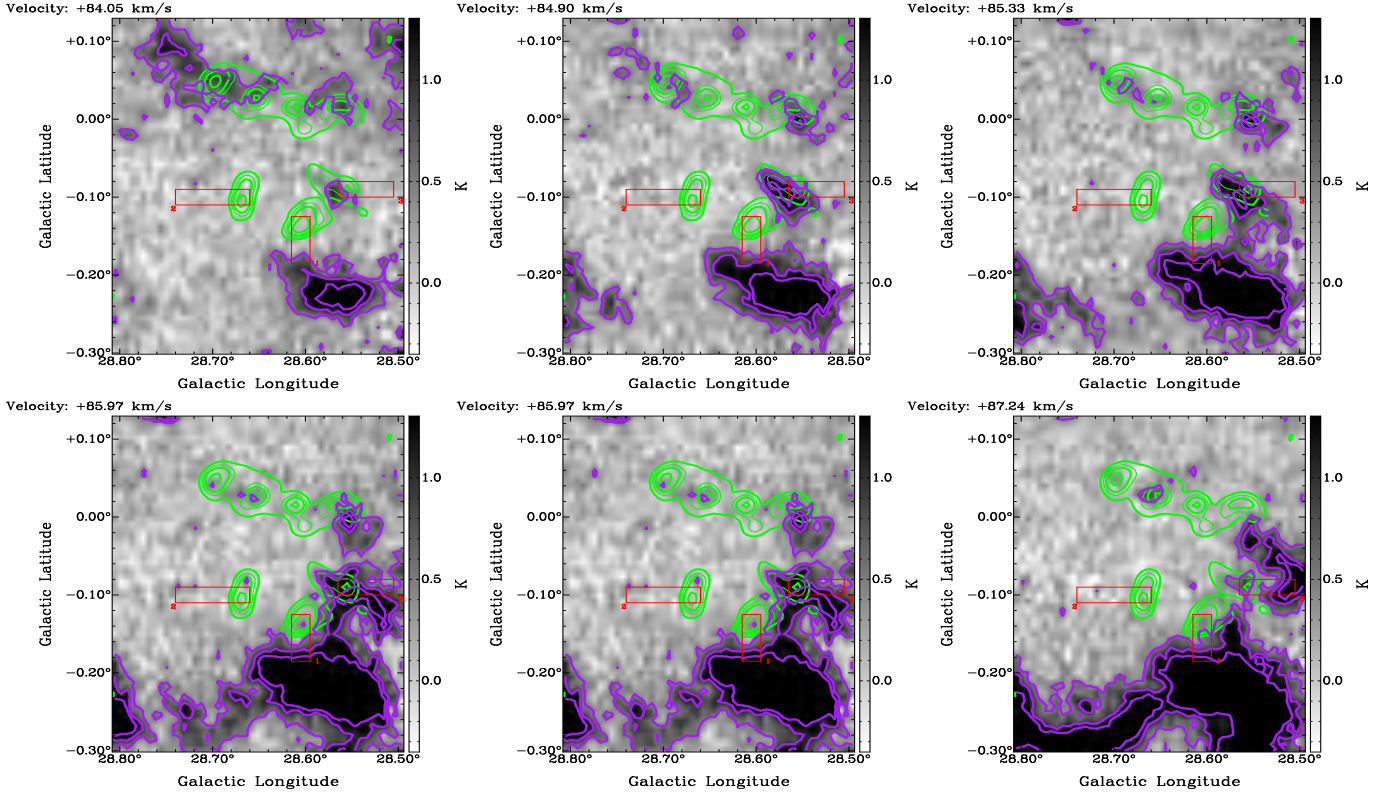


**Figure 12.** G28.6 – 0.1  $^{13}\text{CO}$  channel maps +84.05 to +87.24  $\text{km s}^{-1}$ . The  $^{13}\text{CO}$  contour levels (purple) are at 0.5, 1 and 1.5 K. The continuum contour levels (green) are at 40, 50, 60 and 80 K.

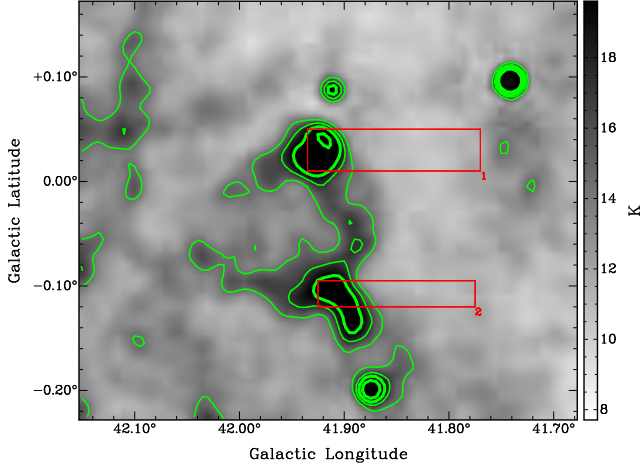


**Figure 13.** 1420 MHz continuum image of SNR G42.0 – 0.1 (left side of top red box) and nearby HII region (left side of lower red box). The contour levels (green) are at 14.5, 17, 20 and 25 K.

given by  $R = 12.9\text{pc}(\epsilon_0/n_0)^{1/5}t_4^{2/5}$ , where  $\epsilon_0$  is the explosion energy in units of  $0.75 \times 10^{51}\text{erg}$ ,  $n_0$  is the interstellar medium density in units of  $\text{cm}^{-3}$ , and  $t_4$  is the SNR age in units of  $10^4\text{yr}$ .

We use a mean explosion energy of  $5 \times 10^{50}$  erg, which was found for Large Magellanic Cloud SNRs by Leahy (2017). An ISM density of  $1 \text{ cm}^{-3}$  is used. We note that the radius is sensitive to the  $1/5$  power of energy/density, and age is sensitive to the  $1/2$  power of energy/density, so that the estimates depend weakly on the energy and density assumptions.

The mean angular radius of each SNR, measured from the 1.4 GHz radio continuum image, is 3.6 arcmin for G20.4 + 0.1, 9 arcmin for G24.7 – 0.6, 5.5 arcmin for G28.6 – 0.1 and 1.8 arcmin for G42.0 – 0.1. Using our distances, we obtain shock radii  $R=7.9$  pc for G20.4 + 0.1,  $R=9.9$  pc for G24.7 – 0.6,  $R=15.4$  pc for G28.6 – 0.1 and  $R=1.8$  pc for G42.0 – 0.1. The resulting age estimates from the Sedov model for the four SNRs, respectively, are 3640 yr, 6400 yr, 19000 yr, and 100yr. Because the age for G42.0 – 0.1 is unrealistically small, our estimate of explosion energy or of interstellar medium density must

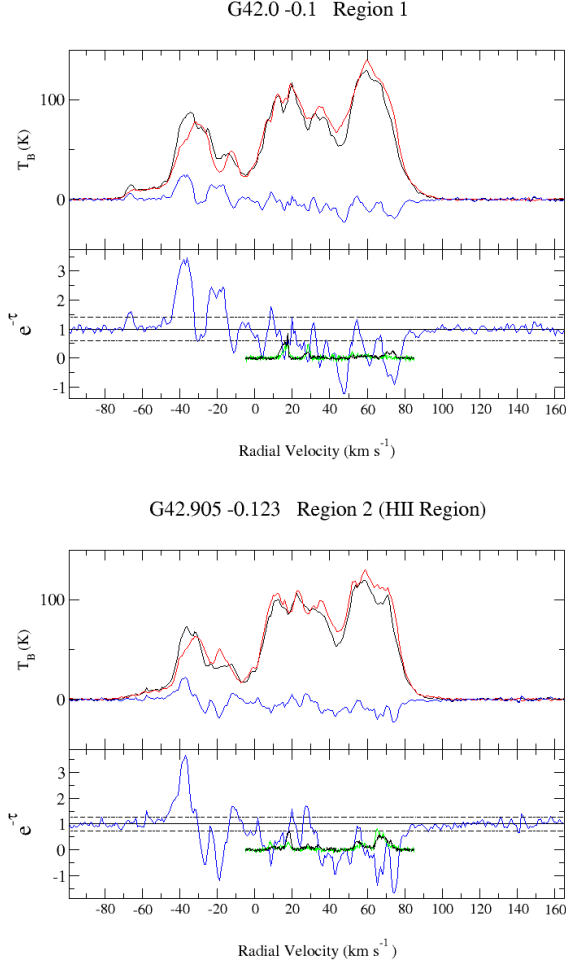


**Figure 14.** G42.0 – 0.1 spectra: The top two panels are for Region 1, the lower two panels are for Region 2. The top panel in each pair shows HI emission spectra: source spectrum (black), background spectrum (red) and difference (blue). The bottom panel in each pair gives the HI absorption spectrum (blue), the  $^{13}\text{CO}$  source spectrum (green) and the  $^{13}\text{CO}$  background spectrum (black). The dashed line is the  $\pm 2\sigma$  noise level of the HI absorption spectrum.

be incorrect. To obtain such a small radius as 1.8 pc, the value of  $(\epsilon_0/n_0)$  must be significantly smaller. E.g. a factor 100 decrease in  $(\epsilon_0/n_0)$  increases the estimated age by a factor of 10 to a more realistic 1000 yr. Because of the very wide range of densities in the interstellar medium, it is more likely that the density is higher by a factor of 100 than the explosion energy lower by a

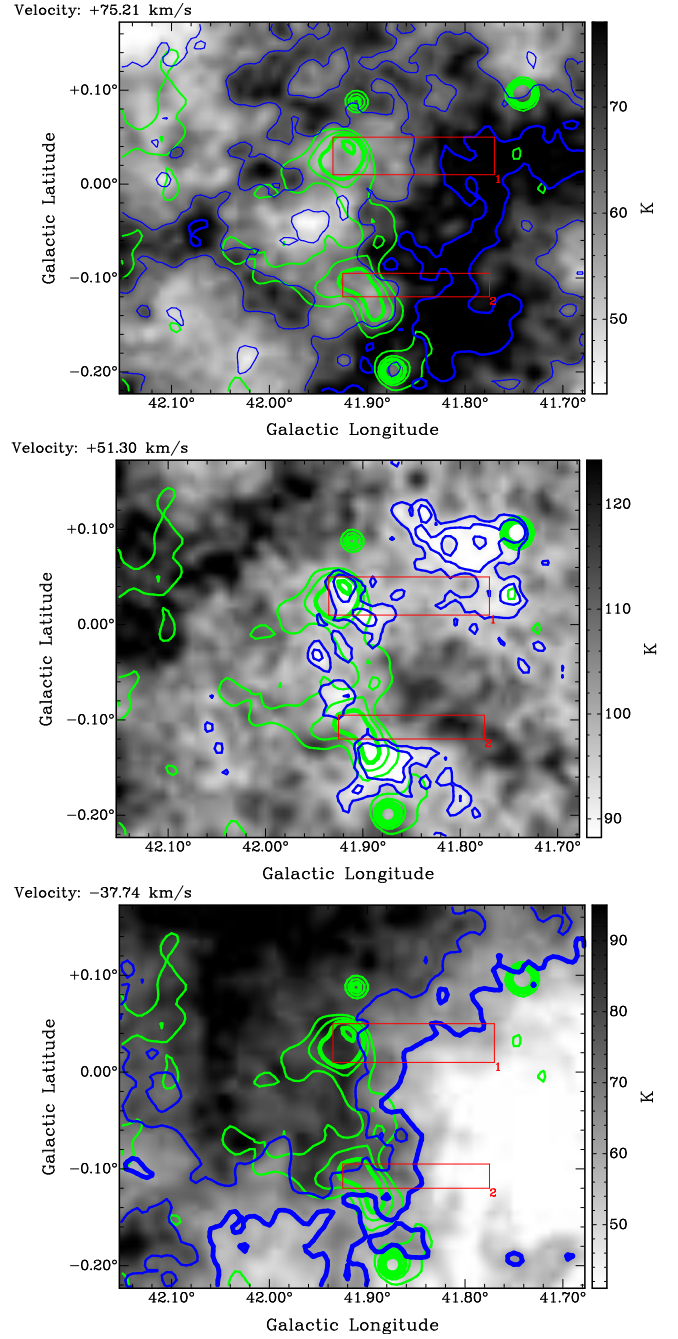


**Figure 15.** G24.7 – 0.6 HI channel maps at +75.21 (top), +51.30 (middle) and  $-37.74 \text{ km s}^{-1}$  (bottom). The HI contour levels (Blue) are at 50, 65 and 60 K for the +75.21 channel map, 90 and 95 K for the +51.30 channel map and 60 & 75 for the  $-37.74$  channel map. The continuum contour levels (green) are at 20, 25, 30 and 35 K.



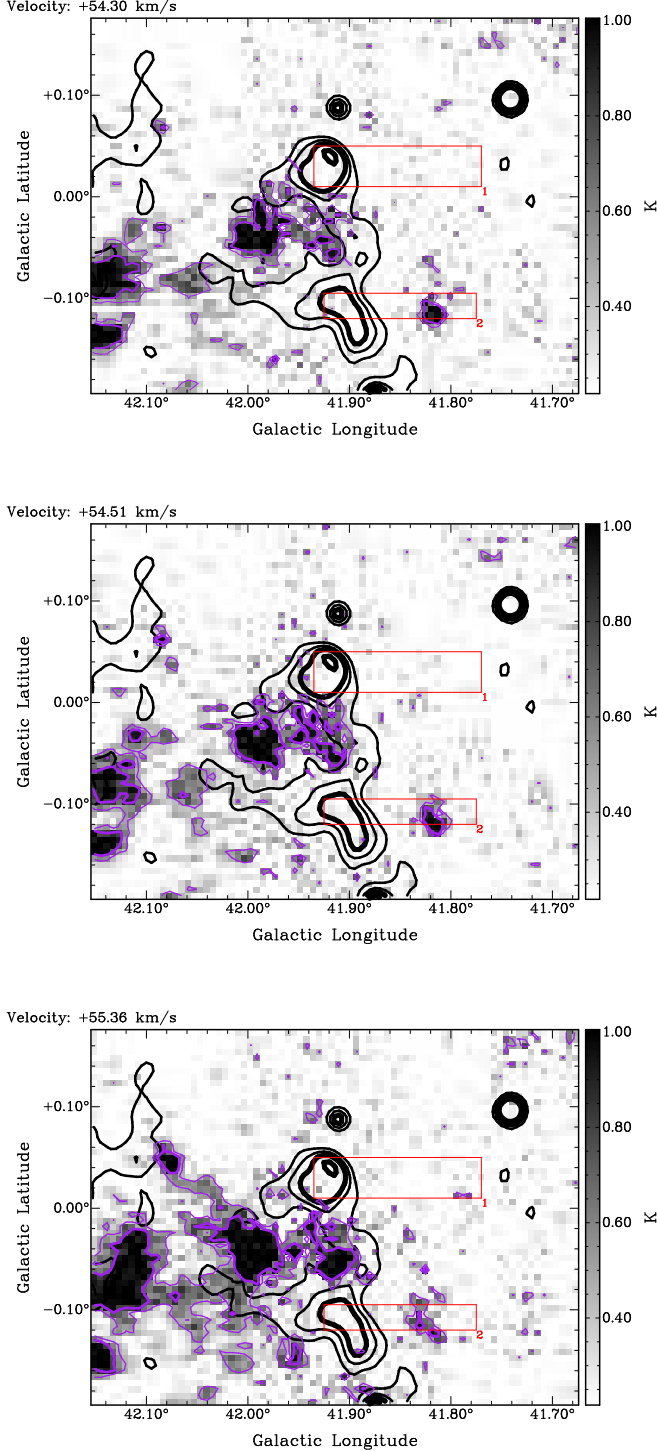


**Figure 16.** G42.0-0.1  $^{13}\text{CO}$  channel maps +54.30 to +55.15  $\text{km s}^{-1}$ . The  $^{13}\text{CO}$  contour levels (purple) are at 0.5 and 0.8 K. The continuum contour levels (black) are at 14.5, 17, 20 and 25 K.

factor of 100. G42.0 - 0.1 is small enough that it is probably a very young SNR, so that the Sedov phase is not applicable to it. Until more detailed observations of this SNR are available, a reliable estimate of its age cannot be made.

In this work, we analyse HI spectra,  $^{13}\text{CO}$  spectra, HI channel maps and  $^{13}\text{CO}$  channel maps of four SNRs in the VGPS survey area. These SNRs do not have previous distance measurements, except for G28.6 - 0.1 which has an estimate based on X-ray column density. For each of the SNRs a probable molecular cloud association is found, based on morphological match of the SNR boundary with the molecular cloud boundary. We find distances to the SNRs G20.4 + 0.1, G24.7 - 0.6, G28.6 - 0.1 and G42.0 - 0.1 as  $7.8 \pm 0.2$  kpc,  $3.8 \pm 0.2$  kpc,  $9.6 \pm 0.3$  kpc and  $3.5 \pm 0.4$  kpc, respectively. From a Sedov model we estimate the ages of the SNRs and find the first three are middle aged SNRs ( $\sim 4000$  to  $20,000$  yr old) but that G42.0 - 0.1 is small angular diameter and likely young ( $\sim 1000$  yr).

## ACKNOWLEDGEMENTS

This work was supported in part by a grant from the Natural Sciences and Engineering Research Council of Canada.



**Table 1.** Distances to supernova remnants

#	Source	Previous Distance(kpc)	Reference	$V_r$ km s <sup>-1</sup>	KDAR <sup>1</sup>	New Distance (kpc)
3.1	G20.4 +0.1	-	-	~ 120	TP	$7.8 \pm 0.2$
3.2	G24.7 -0.6	-	-	60.67	N	$3.8 \pm 0.2$
3.3	G28.6 -0.1	$6 - 8.5$ <sup>2</sup>	Bamba et al. (2001)	86	F	$9.6 \pm 0.3$
3.4	G42.0 -0.1	-	-	55.15	N	$3.5 \pm 0.4$

Notes:

1. KDAR- Kinematic Distance Ambiguity Resolution, indicating whether the SNR is at the near (N), far (F) or tangent point (TP) distance.
2. From X-ray column density.

## REFERENCES

- Alves, M. I. R., Davies, R. D., Dickinson, C., et al. 2012, MNRAS, 422, 2429
- Bamba, A., Ueno, M., Koyama, K., & Yamauchi, S. 2001, PASJ, 53, L21
- Brogan, C. L., Gelfand, J. D., Gaensler, B. M., Kassim, N. E., & Lazio, T. J. W. 2006, ApJL, 639, L25
- Clark, D. H., Caswell, J. L., & Green, A. J. 1975, Australian Journal of Physics Astrophysical Supplement, 37, 1
- Cox, D. P. 1972, ApJ, 178, 159
- Dubner, G. M., Moffett, D. A., Goss, W. M., & Winkler, P. F. 1993, AJ, 105, 2251
- Green, D. A. 2014, Bulletin of the Astronomical Society of India, 42, 47
- Helfand, D. J., Velusamy, T., Becker, R. H., & Lockman, F. J. 1989, ApJ, 341, 151
- Jackson, J. M., Rathborne, J. M., Shah, R. Y., et al. 2006, ApJS, 163, 145
- Kaplan, D. L., Kulkarni, S. R., Frail, D. A., & van Kerkwijk, M. H. 2002, ApJ, 566, 378
- Koo, B.-C., & Heiles, C. 1991, ApJ, 382, 204
- Kwee, K. K., Muller, C. A., & Westerhout, G. 1954, BAN, 12, 211
- Leahy, D. A. 2017, ApJ, 837, 36
- Leahy, D., & Tian, W. 2010, The Dynamic Interstellar Medium: A Celebration of the Canadian Galactic Plane Survey, 438, 365
- Lockman, F. J., Pisano, D. J., & Howard, G. J. 1996, ApJ, 472, 173
- Persic, M., Salucci, P., & Stel, F. 1996, MNRAS, 281, 27
- Quireza, C., Rood, R. T., Bania, T. M., Balser, D. S., & Maciel, W. J. 2006, ApJ, 653, 1226
- Ranasinghe, S., & Leahy, D. A. 2017, ApJ, 843, 119
- Reid, M. J., Menten, K. M., Brunthaler, A., et al. 2014, ApJ, 783, 130
- Stil, J. M., Taylor, A. R., Dickey, J. M., et al. 2006, AJ, 132, 1158